Synchrotron radiation photoemission spectroscopy of III-VI compounds

G. Margaritondo,* J. E. Rowe, and S. B. Christman
Bell Laboratories, Murray Hill, New Jersey 07974
(Received 24 November 1976)

The valence and conduction bands of GaSe, GaS, and InSe have been studied with several synchrotron-radiation photoelectron-spectroscopy techniques. Energy distribution curves (EDC's) in the photon energy range 16–36 eV show four main valence-band density of states features between the top of the valence band and the cation d core levels. The nature of these features is discussed in terms of the two kinds of intralayer chemical bonds, cation-cation bonds and anion-cation bonds. Photon polarization effects show that the top of the valence band has a p_z-like character and this character extends to lower energies for GaS than for GaSe and InSe. Photon-energy effects reveal a fine structure of most valence-band features which is particularly pronounced for InSe. Constant-initial-state (CIS) spectra have been taken employing several EDC peaks as initial states. Most of the CIS data can be straightforwardly interpreted in terms of the conduction-band density of states. Good agreement is found with pseudopotential band-structure calculations for GaSe and a direct interpretation is derived for the observed features in the reflectivity spectra.

The recent introduction of storage rings as ultraviolet photon sources has considerably expanded the information that photoemission spectroscopy can provide.[1] The number of photoelectrons emitted per unit time within a small solid angle and a small energy range is a function of many variables, such as electron kinetic energy (E), k-vector direction,[2] electron-spin polarization,[3] photon energy ($\hbar\omega$), direction of incidence,[4] and photon polarization.[5,6] In most previous experiments, limitations of the photon source have confined the experiments to the electron-energy dependence. This situation is now changing and many new photoemission-spectroscopy techniques have been introduced[5-9] that go beyond the traditional energy distribution curves (EDC's). Photon-energy and polarization effects of the EDC's[5,6] provide information on the optical transition probability and the electronic state symmetry. A more complete picture of the valence-band density of states is obtained in this way. Constant-initial-state (CIS) spectra[8] reveal the conduction-band density of states features above the vacuum level by synchronously varying the photon energy and electron energy. Using both EDC and CIS techniques one can obtain extensive information on the electronic properties of solids and solid surfaces for energies above and below the Fermi level.

Semiconducting III-VI compounds offer many advantages for such an investigation. Their layered structure confines the study to two-dimensional k-vector and real spaces to a first approximation[10-12] thus simplifying both theory and experiment. The electronic properties are described equally well in terms of bands or chemical bonds. Optical data are available over a large spectral region for some of the compounds.[13-18] These optical data connect the two energy regions that we have studied with photoemission techniques, i.e., below the Fermi energy and above the vacuum level. The present investigation has been extended to three materials: GaSe, GaS, and InSe. The structure of a layer (see Fig. 1) is the same for all of them and consists of four sheets of hexagonal-close-packed atoms with anion sheets on the outside of the layer and cation sheets inside. The number of filled bands per layer is relatively large and this makes the band-structure picture more complicated than a chemical-bond description of electronic structure since there are only two kinds of intralayer bonds (cation-cation bond and anion-cation bond). The Brillouin zone (Fig. 2) has a hexagonal two-dimensional projection and the nearest-neighbor atomic configuration is trigonal.

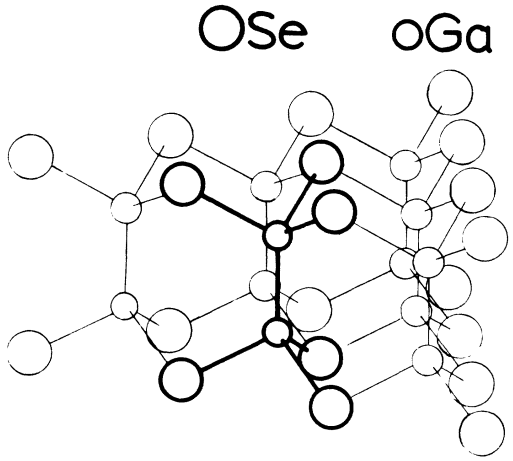

FIG. 1. Lattice structure of GaSe, GaS, and InSe.

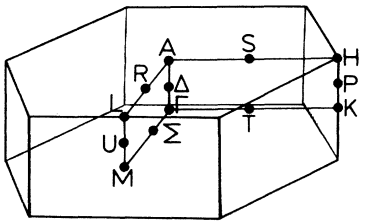

FIG. 2. Three-dimensional Brillouin zone of GaSe, GaS, and InSe.

Only minor differences among the results for different materials were expected *a priori* because the crystal structure is similar for all of them even if there are differences in the stacking geometry. Nevertheless we find that some experimental differences are quite marked and follow in different materials the same trend as other physical properties such as the interband transition energies.

Details of the experimental procedure are given in Sec. II. The experimental results are reported and discussed in Secs. III and IV which deal with polarization-dependent EDC's and CIS spectra, respectively. In these sections, our results are compared with information from other sources such as theory[10-12] and optical spectroscopy.[13-18] We anticipate that some of our results can be understood on the basis of recent pseudopotential band-structure calculations,[12] but most of them are still beyond the available theoretical data. Such is the case for example of the angle-dependent InSe spectral fine structure that will constitute a severe k-dependence test of future theoretical wave functions. In Sec. V, general conclusions and comments are reported.

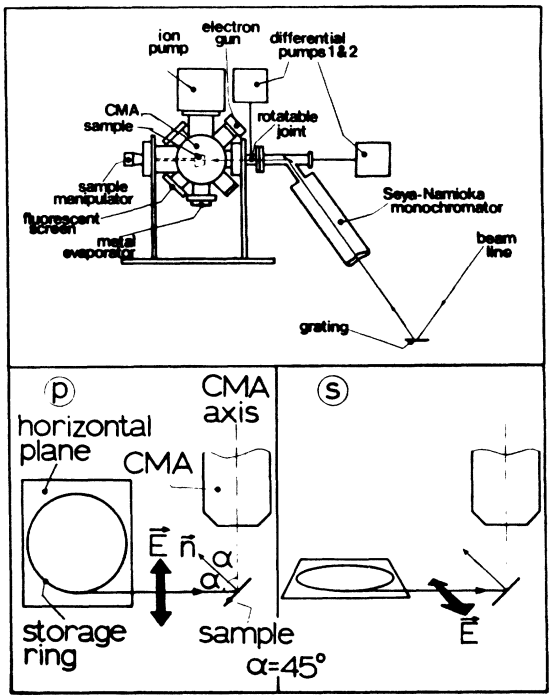

FIG. 3. *Upper half*: schematic of the experimental chamber. *Lower half, left*: configuration for p-polarized photons. *Lower half, right*: configuration for s-polarized photons. The collection geometry and the angle of incidence are the same for both configurations. The differentially pumped rotatable joint (see upper half of the figure) connects the sample chamber to the monochromator. This allows switching between the two configurations without breaking the ultrahigh vacuum.

II. EXPERIMENTAL PROCEDURES

The experimental procedure consisted of taking EDC's at several photon energies and CIS data for several initial-state energies on the clear surface of a cleaved sample under ultrahigh vacuum conditions. The EDC's and the CIS curves were taken for two different photon polarizations without changing the collection geometry in order to avoid spurious geometrical effects.

The experimental work has been performed at the University of Wisconsin Storage Ring. The beam line was equipped with a bakeable vertical Seya-Namioka monochromator and several horizontal reflections in the optical system raised the synchrotron radiation polarization factor to >98%. The exit slit of the monochromator was connected to the experimental chamber through a differentially pumped rotatable joint (see Fig. 3: upper half). This allowed one to rotate the entire experimental chamber by 90° around the beam line without breaking the ultrahigh vacuum. During the rotation the rise in pressure was below a factor of 4 from the base value ~5×10^{-10} Torr. The purpose of this rotation was to switch from one to the other of the two configurations illustrated by the lower half of Fig. 3. For both configurations the beam line and the axis of the cylindrical-mirror electron-energy analyzer (CMA) were perpendicular to each other and the sample normal was at 45° with respect to both of them. In this way, the *photon polarization* changed with the configuration, but the collection geometry was the same for both configurations since sample and CMA were rigidly connected to each other. The electric vector was parallel to the plane of incidence (p polarization) in the left configuration of Fig. 3 and perpendicular (s polarization) in the right one. The above pro-

cedure enabled us to separate *real* photon polarization effects from spurious *geometrical* effects. This would have not been achieved while simply rotating only the sample since strong photoemission angular effects have been observed for these materials.[19-21]

The surfaces of the samples cleaved under UHV conditions were fairly stable and the experimental results did not change over a period of several days under the best pressure conditions. As above mentioned, we have explored the dependence of the photoemission intensity on several variables. In our angle-integrated collection geometry once one of the configurations of Fig. 3 has been selected one can regard the number of collected photoelectrons, N, as a function of E and $\hbar\omega$. The functional surface $N=N(E,\hbar\omega)$ can be swept in an infinite number of different ways. We chose to sweep it either along a line $\hbar\omega=\text{const}$ (EDC mode) or along a line $E-\hbar\omega=E_i=\text{const}$ (CIS mode).[8,9] In the first mode, EDC's were recorded for several photon energies in the range $\hbar\omega=16-36$ eV. Peaks in these spectra could be correlated with the valence-band density of states and the basic spectral shape almost completely converged towards the density-of-states limit at high photon energies $\hbar\omega>28$ eV. In the second mode, we expected the spectral features to be mostly related to the final state of the optical transition. Indeed, the initial-state energy is constant and equal to the selected E_i for each CIS spectrum unless Auger processes or direct recombination processes take place.[9] Moreover the initial state energy E_i was selected to coincide with one of the EDC peaks. This corresponds to a flat energy versus k-space dispersion of the initial state, i.e., $\nabla_{\vec{k}}E_i=0$. Thus, the energy distribution of the joint density of states is large and does not depend too much on the initial state. From the experimental point of view, the CIS mode required the stepping motor moving the Seya-Namioka monochromator grating to be driven by a pulse generator. The monochromator had an analog wavelength output which was digitally processed to obtain an analog CMA control signal which is proportional to $E_i+\hbar\omega$.

A third geometry not appearing in Fig. 3 has been used to study collection geometry effects on the spectra. This geometry is shown in the inset of Fig. 8 and consisted of having the beam line perpendicular to the CMA axis and to the sample surface. The azimuthal angle ϕ could be varied by rotating the sample around its normal. We point out that in this case as well as for the s configuration of Fig. 3 the electric vector of the radiation had *no components perpendicular to the sample surface* (i.e., $E_z=0$).

III. ENERGY DISTRIBUTION CURVES AND PHOTON POLARIZATION EFFECTS

The aim of this article is to provide a picture of the electronic states of GaSe, GaS, and InSe over a large energy range as schematically illustrated by Fig. 4. Here the valence band is represented in first approximation by an EDC taken at $\hbar\omega=28$ eV and the conduction band by a CIS spectrum having peak E in the EDC for initial state. In the present section, we shall discuss in detail the EDC's while CIS data will be analyzed in Sec. IV. We shall see that the four main EDC features are closely related to the valence-band density of states and that a p_z-like character is exhibited by the top of the valence band over an energy region whose extension depends on the energy gap and lattice constant of the material. A fine structure which is not yet clearly understood was observed for several spectral peaks and will be discussed at the end of this section.

Although EDC's similar to that of Fig. 4 have been published by several authors for GaSe,[5,22] the large number of spectral features and their closeness in energy has caused some controversy about a detailed identification. We would like to show that this controversy can be resolved at least in part by studying photon energy and polarization effects on the EDC's and that more information can be obtained by comparing the results for several different III-VI compounds than by studying only a single material. The atomic orbitals contributing to the valence band are 4s and 4p from Ga, 5s and 5p from In, 4s and 4p from Se, and 3s and 3p from S. The anion s levels are confined at rather low energies and appear as a weak broad band at ~10–14 eV from the top of the valence band E_v in some of the EDC's.[5,22] The

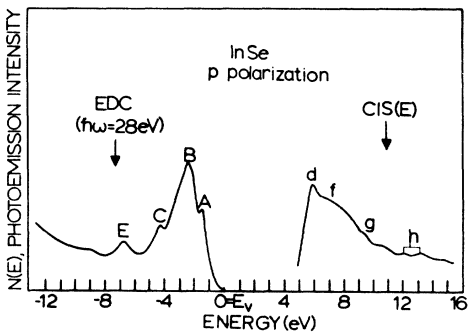

FIG. 4. Combining EDC and CIS modes allows the study of both valence and conduction bands. Both spectra are for InSe and p-polarized photons. EDC taken at $\hbar\omega=28$ eV. CIS spectrum has peak E in the EDC for initial state. The structure labeling is explained in the text.

remaining orbitals occur in the energy range from the top of the valence band down to 8–10 eV from E_v.[5,22] The p-like cation and anion orbitals are expected at higher energies than the cation s orbitals. The theory[11,12] indicates that the latter should give several density-of-states peaks with bonding and antibonding Ga–Ga character, respectively. These two peaks are expected at 3–8 eV from E_v. The p-like orbitals are in the top of the valence bands and participate to both kinds of bonds. In this energy region, photon polarization effects are most helpful to identify the orbital symmetry.

Figure 5 reports GaSe EDC's taken at $\hbar\omega = 20$, 24, 28, and 32 eV for both polarizations. The labeling of the structure is that most widely employed in the literature.[5,22] The energy position of peaks A and C does not change with $\hbar\omega$. Some dispersion is observed for peaks B and E. The $\hbar\omega = 24$ eV, p-polarization EDC clearly shows a doublet fine structure of peak B. In the other spectra the relative weight of the two components of this doublet explains the shift of peak B center of gravity with $\hbar\omega$. This effect is also present in the s-polarization EDC's where the high-energy component of peak B is in general weaker than for p-polarization. Comparison of s- and p-polarization EDC's of Fig. 5 clearly shows that a much stronger polarization effect is present for peak A. Quantitative understanding of this effect would require a detailed calculation of the transition probabilities, i.e., a good knowledge of the initial- and final-state wave functions. The present theoretical knowledge of the conduction-band wave functions is not good enough for this. However, the remarkable strength of the observed polarization effects allows identification of the initial-state symmetry from the following qualitative arguments. As already mentioned, mostly p-like

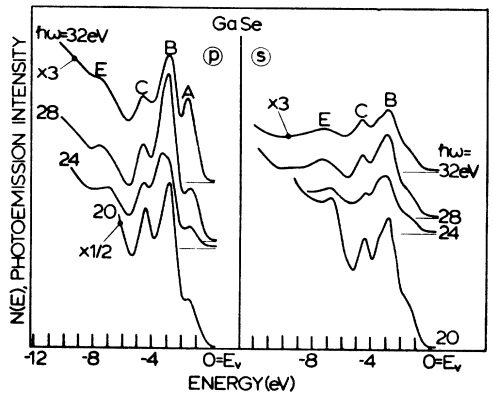

FIG. 5. GaSe EDC's taken at four photon energies ($\hbar\omega = 20$, 24, 28, and 32 eV) and with both polarizations. Spectra normalized to the photon flux.

orbitals are expected in the energy region of peak A.[11,12] Thus, the final state of the optical transition can be either s- or d-like. In the s configuration of Fig. 3, one has $E_z = 0$ and dipole transitions to an s-like final state are only allowed from p_x, p_y initial states. Thus, peak A originates from p_z-like initial states if the final state is s-like. The situation is more complicated for d-like final states. No strong polarization effects are expected in this case unless the final state only contains one particular kind of d orbitals. The observed polarization effects could correspond in the latter case either to a marked p_z or to a marked p_x, p_y initial-state character for d_{z^2} and d_{xz}, d_{yz} final states, respectively. The second of these two interpretations is weak since all calculations predict the p_z-like states at higher energies than the p_x,p_y ones.[5,11,12] Moreover the observed polarization effect is qualitatively constant over the range $\hbar\omega = 18$–36 eV. Prevalence over such a wide energy region of a peculiar kind of d orbital in the final state is unrealistic. Thus, the conclusion that for peak A the initial state has prevalent p_z-like character appears independent of the final-state character. The above analysis is of course a first approximation since here we are dealing with bands rather than atomic orbitals. Moreover the possible rapid space variations of the local electric field can reduce the validity of the dipole approximation. The removal of all these approximation would *weaken* the above selection rules. This explains why peak A does not completely disappear in the s configuration, but the polarization effect for peak A is still so strong that the above analysis is basically correct. A p_z-like character of the top of the valence band is in agreement with angle-dependent x-ray-photoemission-spectroscopy results[23] and with theoretical predictions.[10,12] Peak A is essentially bonding Ga–Ga states containing Ga p_z orbitals mixed with some nonbonding Se p_z orbitals (π bands). These bonding states and the corresponding Ga–Ga antibonding ones form the GaSe energy gap. The identification of the p_z character of peak A makes analyzing the remainder of the valence band easier. Both the energy position and the intensity of peak B confirm the theoretical identification[11,12] of p_x,p_y states of the Ga–Se bond. However, its polarization-dependent doublet structure indicate that some p_z character is also present and decreases at larger binding energies. The nature of peak C is rather controversial. The theory predicts the states responsible for peak B to also give a second feature at slightly larger binding energies,[12] but the theoretical energy separation between this feature and peak B is smaller than the experimental separation between peaks

B and C. The gap present in the spectra between peaks E and C would suggest that these are the above mentioned Ga–Ga bonding and antibonding states containing Ga s orbitals.[11,2] Recent polar-angle resolved photoemission data solve this controversy[20,21] in the following way. In an angular-integrated geometry we mostly collect electrons with large polar angles, i.e., whose initial and final states are far from the Γ point in the two-dimensional reduced zone. The experimental band structure[21] obtained from angle-resolved UPS clearly show that in these k-space regions peaks B and C have similar nature while the opposite is true close to the Γ point. Thus, in our spectra peak C mostly originates from p_x, p_y states in the Ga–Se bond while peak E must be identified as due to states with antibonding Ga–Ga character. Its bonding partner is also observed at lower energies in the angle-resolved spectra,[21] but the two peaks are not resolved in our angle-integrated spectra. Between these peaks and the anion s-states another peak (F) whose origin is not clear is present in some cases.

The GaS EDC's of Fig. 6 show that the similarities between different III-VI compound with the same crystal structure are not as extended as one could expect. The general spectral sequence of the valence-band features is the same for GaS as for GaSe, but peaks A and B are now *both* polarization dependent. The weak p_z-like contribution found in peak B for GaSe is thus enhanced for GaS. Also, we observe that the doublet fine structure of peak B is now almost absent although one still observes some of the $\hbar\omega$ dispersion it causes.

The InSe EDC's of Fig. 7 also show a general similarity with GaSe, but differences are present in the opposite sense with respect to those found between GaSe and GaS. The polarization effect for peak B is at least as weak for InSe as for GaSe and that for peak A is more pronounced. Thus the p_z-like character is confined at higher energies for InSe than for GaSe. The doublet fine structure of

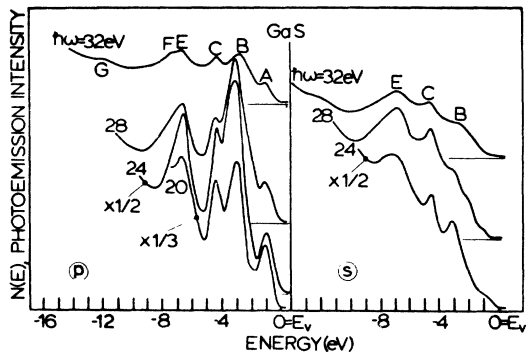

FIG. 6. GaS EDC's. Normalization as for Fig. 5.

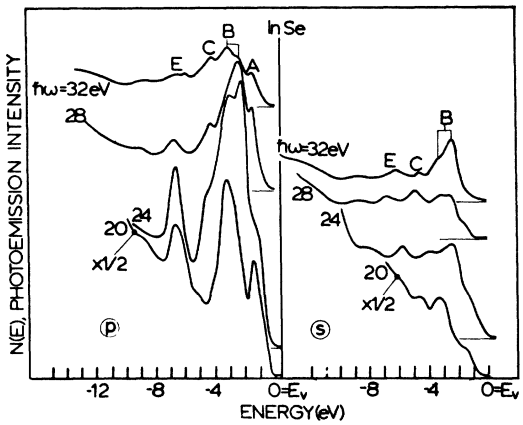

FIG. 7. InSe EDC's. Normalization as for Fig. 5.

peak B is more pronounced than for GaSe and so is its dependence on photon energy and polarization. A doublet character is also observed for peaks E and C. Both components of peak E doublet are present in the $\hbar\omega = 32$ eV, p-polarization spectrum of Fig. 7 and either one or the other of the two components of the doublet prevails in each of the remaining spectra. The $\hbar\omega$ dependence of peak E fine structure is shown in the right-hand side of Fig. 8. The complete intensity reversal between the two components while $\hbar\omega$ increases is probably due to matrix-element effects since we shall see that the conduction-band density of states has a rather smooth energy dependence at these values of $\hbar\omega$. For peak C, a doublet character is indicated by its large dispersion with $\hbar\omega$ in the spec-

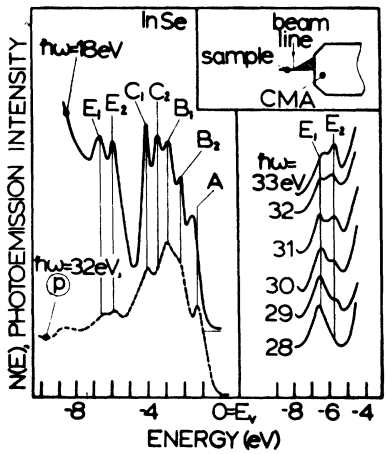

FIG. 8. The InSe EDC fine structure is emphasized by the collection geometry shown in the inset. *Left*: the $\hbar\omega = 28$ eV EDC taken in this geometry, shown as a solid line is compared to the $\hbar\omega = 32$ eV EDC taken with the p configuration of Fig. 3, shown as a dashed line. *Right*: $\hbar\omega$ dependence of the peak E fine structure observed for InSe in the p configuration of Fig. 3. These spectra have been vertically shifted for clarity.

TABLE I. Average valence band structure positions.[a]

Peak[b]	GaSe	GaS	InSe
A	1.3–1.4	1.0	1.2–1.5
B_1, B_2	3.5, 3.0	3.2	3.0–3.2, 2.2–2.4
(C_0), C_1, C_2	4.6	4.4	(4.7), 4.1, 3.5
E_1, E_2	7.2–7.4	6.9	6.5–6.7, 4.8–6.0
F	9.3–9.5	7.8–8.2	9.0
d-core level cation doublet	18.8	18.8	16.9, 17.7

[a]All energies in eV, measured from E_v. The uncertainty is ± 0.2 eV unless it has been increased by $\hbar\omega$ dispersion, in which case an energy range is given rather than a point.

[b]Notice that the fine structure of peaks B, C, E and of the d-core level is only resolved for InSe and in the case of peak B for GaSe.

tra of Fig. 7. The fine structure of the InSe EDC's features is much more pronounced in the spectra taken with the third experimental geometry described at the end of experimental section and shown by the inset of Fig. 8. One of these spectra is reported in Fig. 8 (see the left-hand side: solid line). Comparison of different spectra shows that *three* different structures are present in the C-peak region. Two of them, C_1 and C_2, appear in Fig. 8 while the third one C_0 appears at slightly lower energy ~-4.7 eV in the $\hbar\omega = 28$ eV spectra of Fig. 7.

Table I summarizes the energy position of the valence-band density-of-states structures for the three samples. We have seen that pronounced differences are found among the results for different materials even if the energy positions of Table I are quite similar. These differences follow the same trend of other physical properties. The interband optical-transition energies E_0, E_1, E_3 increase in the sequence InSe, GaSe, GaS while the cation-anion bond length decreases.[24] In this same sequence, the polarization effects are less confined to a region close to E_v and the fine structure of the peaks is less pronounced and less $\hbar\omega$-dependent. The differences among the materials appear related to the length of the cation-anion bond. A relation to the cation-cation bond is less direct since this bond is anomalously large for InSe and it has been suggested[24] that this is indirectly due to the charge transfer between In and Se. Considering the nature of peaks B and C a relation with the Ga–Se bond is quite understandable for all the differences we find among the materials, but for the pronounced fine structure of peak E in InSe. This suggests that the observed fine structure has different origin for different peaks. The 0.4–0.8 eV energy splitting of peak B for InSe can be compatible with a solid-state-enhanced spin-orbit splitting of Se $4p$ and In $5p$ since the atomic splittings are 0.37 and 0.27 eV, respectively. This would explain the smaller splitting for Ga compounds since the atomic Ga $4p$ splitting is 0.12 eV. A spin-orbit splitting cannot easily explain the fine structure of peak E which at least for GaSe mostly contain s-like states and for peak E a crystal-field splitting is probably present. We point out that the results of Fig. 8 (see left) indicate that the reproduction of the observed fine structure by future theoretical calculations will critically depend on the way the Brillouin zone will be sampled. Thus the fine structure should become, in the future, a sensitive probe for the k dependence of theoretical wave functions.

IV. CONDUCTION BAND SPECTRA

A detailed analysis of several different CIS curves shows that at least four main structures are present for all the three materials in the conduction-band density-of-states region above the vacuum level and up to ~16 eV above E_v. Several more structures are found only for some of the materials. The results are in good agreement with theory and optical data.

The CIS data we obtain show that the III-VI materials we study are almost ideal for this technique. As discussed in Sec. II we expect our experimental procedure to emphasize the final state effects in the CIS spectra. The nature of CIS spectral structures can be checked *a posteriori* since the final-state-related features must be at constant electron kinetic energy in different spectra rather than at constant photon energy.[8] Indeed this is what we find for the majority of the spectral features. The conduction-band density of states of these materials appears particularly rich in structure. The theory[12,25] shows that for GaSe the conduction band has molecular character at least up to 10–14 eV above E_v. The wave functions are localized in space and this corresponds to more structure in the conduction band density of states than for group IV or III-VI semiconductors. Analyzing the experimental data in terms of the final density of states is of course an approximation. As we shall see below, this does not affect too much the determination of the position in energy of conduction-band features. Some caution must be used while analyzing the intensity of the spectral features since in the low-photon-energy region the intensity is influenced by the secondary electrons' background and by the increase of the oscillator strength while $\hbar\omega$ decreases. Therefore comparing the relative intensity of different low-photon-energy features is not too meaningful un-

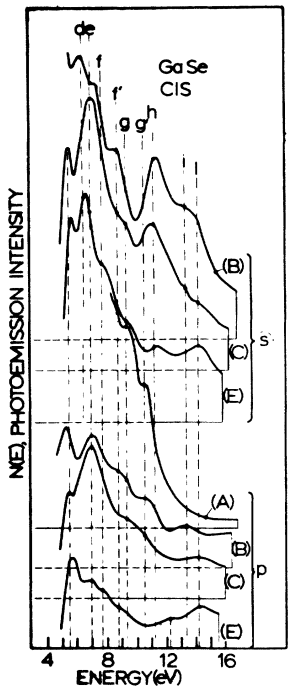

FIG. 9. GaSe CIS spectra for four different initial states, peaks A, B, C, and E in the EDC's, and both photon polarizations. The spectra have been shifted in energy to obtain alignment of the constant-final-state-energy structures, and normalized to the monochromator response and to the synchrotron current. The structure labeling is commented in the text.

less they are close in energy to each other.

Figure 9 reports GaSe CIS spectra taken for several different initial states in both photon polarizations. The first structure around 5.5 eV above E_v is spurious and due to the vacuum-level threshold at ~5.3–5.4 eV. Nine conduction-band structures are observed in the energy region between 6–15 eV above E_v. At higher energies, all spectra become much flatter and this corresponds to a nearly plane-wave final-state character for most transitions analyzed in Sec. IV.[26] The conduction-band features have been labeled in Fig. 8 as d–l, reserving a, b, c to the three density-of-states peaks below the vacuum level deduced from reflectivity spectra at 2.35, 3.65, and 4.75 eV above E_v.[13] Table II summarizes the average experimental energy position of the conduction-band features and Table III reports the photon energy of the optical transitions in which they participate. As reported in the third column of Table II the presence of the first three features above the vacuum level, d, e, and f, has also been deduced from uv reflectivity data.[13] We point out that CIS spectra provide more information than reflectivity or electron-energy-loss data because absolute energy positions rather than only transition energies are measured. We list in Table III all the optical transitions observed in Fig. 9. Most of these transitions are also observed in reflectivity and energy-loss spectra (see Table III, second and third columns),[13–16] but the previous interpretation was sometimes wrong and quite

TABLE II. CIS results for GaSe.

Conduction band feature	Energy position[a] Present data (average)	From reflectivity (Ref. 13)	Theoretical (Refs. 12 and 25)	Transition energies[b] A p polarization	A s polarization	B p polarization	B s polarization	C p polarization	C s polarization	E p polarization	E s polarization
(Spurious)	5.5	...	...	...	...	...	...	...	...	...	...
d	6.4	6.15	5.8	...	9.4	No	No	No	} 13.2–13.9	No	} 13.2–13.9
e	6.9–7.0	6.9	6.7	...	10.1–10.2	10.1	11.5	11.5		13.9	
f	7.6–7.7	7.2, 7.6	7.5	...	No	No	No	No	14.7	14.8	
f'	8.7	...	...	9.8–9.9	11.4–11.6	} 11.5–12.4	} 13.3–15.1	No	No	15.8	
g	9.3	...	9.4	10.4–10.5	No			} 13.8–15.1	16.3	No	
g'	10.4	...	...	11.5–11.6	No		No		No	No	
h	11.1–11.2	...	11.0	No	14.3	} 13.5–14.3	15.8–16.0	No	18.3	No	
i	13.3	...	...	No	16.2	16.3	17.7–17.9	No	No	No	
l	14.2	...	...	No	No	No	18.9–19.2	18.9	21.2	21.3	

[a] Energy position in eV, measured from E_v. Uncertainty for our data ± 0.2 eV. No reflectivity data are available above 7.6–8 eV nor theoretical data above ~12 eV.

[b] Transition energy in eV. Each column corresponds to a given initial state and to a given photon polarization. Forbidden transitions are listed as "No".

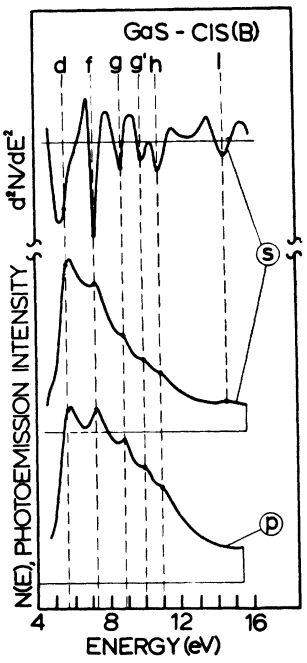

FIG. 10. GaS CIS spectra having peak B for initial state. Normalization as for Fig. 9. The second derivative of the unnormalized s-polarization CIS spectrum (see upper curve) allows a better determination of the structure energy positions.

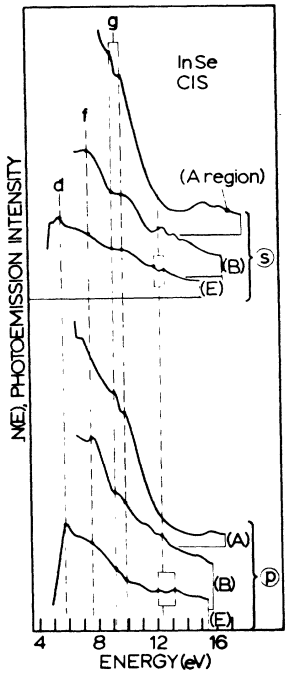

FIG. 11. InSe CIS spectra. Same normalization as for Figs. 9 and 10.

TABLE III. Optical transitions for GaSe.[a]

Transition energy			
CIS (present data)	Reflectivity data	Electron energy loss data	Nature (present data)
9.4	9.3, 9[b]	•••	$B \rightarrow d$
9.8–10.2	•••	•••	$A \rightarrow f'$, $B \rightarrow e$
10.4–10.5	~10.8[c,d]	•••	$A \rightarrow g$
11.4–11.6	•••	•••	$A \rightarrow g'$, $B \rightarrow f'$, $c \rightarrow e$
12.2–12.4	12.3[c]	•••	$B \rightarrow g$
13.2–13.6	13.0[e]	•••	$B \rightarrow g'$, $C \rightarrow f'$, $E \rightarrow d$
13.8–14.3	14.0[c]	•••	$B \rightarrow h$, $C \rightarrow g$, $E \rightarrow e$
14.7–15.1	15.25[c]	•••	$E \rightarrow f$, $C \rightarrow g'$
15.8–16.3	16.4[c]	•••	$B \rightarrow i$, $C \rightarrow h$, $E \rightarrow f'$, $E \rightarrow g$
17.7–17.9	17.6[c]	•••	$C \rightarrow i$
18.3	•••	•••	$E \rightarrow h$
18.9–19.2	18.8[c], 19.5[c]	19.25[f]	$C \rightarrow l$
21.2–2.13	21.27[e], 21.65[c]	21.3[g]	$E \rightarrow l$

[a] Energies in eV; uncertainty for our CIS data ±0.2 eV.
[b] Reference 16.
[c] Reference 13.
[d] Reference 15.
[e] Reference 14.
[f] Reference 27.
[g] Reference 28.

TABLE IV. CIS results for GaS.

Conduction band feature	Average energy position [a] (present data)	Transition energy [a] B (both polarizations)
Spurious d	5.5–5.8	8.8, 9.1
f	7.2–7.3	10.5–10.6
g	8.8	12.1
g'	10.0	13.3
h	11.0	14.3
l	14.6–14.7	17.9–18.0

[a] See the footnote b of Table II.

often it neglected optical processes for whose occurrence we have direct evidence. Some caution is needed while comparing reflectivity data and CIS data since the depth of the sample region sampled is much larger in the former case due to the small electron escape depth. Surfacelike effects can increase the number of allowed optical transitions breaking the dipole bulk selection rules, and this explains why some of our transitions are not seen in reflectivity.[13-16] The fourth column of Table II shows that there is an excellent agreement between the theoretical energy position[12,25] of most conduction-band features and the experimental one from CIS. The agreement extends to all the region where theoretical data are available, up to ~13 eV above the Fermi level, and this is quite remarkable since the theory is based on pseudopotential calculations. A detailed theoretical treatment is not available for the selection rules shown by Table II. A qualitative atomic orbital explanation of these selection rules fails since the prevailing conduction-band character should be p-like up to 9–10 eV above E_v and then d-like.[25] This would imply similar atomic selection rules for most of the final states. The data of Table II show that this is not true, and again prove the molecular character of the conduction band implying that detailed calculations are needed to explain the experimental selection rules. We point out that more differences are present in Table II between the selection rules of the fifth column and the remainders than among the remainders and this again reflects the peculiar p_z-like character of peak A. No other systematic trends can be deduced from Table II.

Figures 10 and 11 show GaS and InSe CIS spectra while Tables IV–VI report the peak positions and transition energies for these materials. The curve on top of Fig. 10 is the second derivative of the GaS s-polarization CIS spectrum shown in the same figure which helps to more carefully determine the energy position of the structures. As one could expect on the basis of the above EDC's, there is a correspondence among the results of Figs. 10 and 11 and those for GaSe. Both the valence- and the conduction-band structures tend to be closer to the energy gap for GaS than for GaSe while no similar behavior for all the structures is found comparing InSe and GaSe. More marked differences among the materials are found for the selection rules. Again, these selection rules show promise of careful checking of future detailed theoretical models. Some qualitative conclusions can be drawn. For example, comparison of Tables II and IV show that there are no forbidden transitions from peak B for GaS, while $B \rightarrow f$ is not allowed for GaSe. This confirms what has already been shown by the polarization effects, i.e., that peak B has in GaS a mixed character less well defined than in GaSe.

V. CONCLUSIONS

Photon-polarization-dependent EDC's and CIS spectra on GaSe, GaS, and InSe are to a large extent explained in terms of valence- and conduction-band density of states, respectively. For both GaSe and InSe, the one has the same binding-en-

TABLE V. CIS results for InSe.

Conduction-band feature	Average energy position [a] (present data)	Transition energy [a] A	B_2		E_2	
		p polarization	s polarization	p polarization	s polarization	p polarization
Spurious d	5.8	•••	•••	•••	11.8	12.0
f	7.6	•••	9.9–10.1	9.9–10.1	13.6	13.8
g	9.1–9.2	10.2	11.7	11.5	15.1	15.3
g'	9.9	10.9	12.4	12.3	16.0	16.0
i	12.3 [b]	No	14.7	14.9	18.9	18.1 [b] / 19.2 [b]

[a] See the footnotes of Table II.

[b] Peak i is a doublet when E_2 is the initial state. The position of the components is 12.0 and 12.8–13.1 eV.

TABLE VI. Optical transitions for InSe.[a]

CIS (present data)	Transition energy Reflectivity (Ref. 15)	Nature (present data)
9.9–10.2	•••	$A \rightarrow g$, $B_2 \rightarrow f$
10.9	10.8	$A \rightarrow g'$
11.5–12.3	•••	$B_2 \rightarrow g$, $B_2 \rightarrow g'$, $E_2 \rightarrow d$
13.6–13.8	•••	$E_2 \rightarrow f$
14.7–15.4[b]	•••	$B_2 \rightarrow i$, $E_2 \rightarrow g$, $E_2 \rightarrow g'$
18.1–19.2	•••	$E_2 \rightarrow i$

[a]See corresponding note for Table III.

[b]A tail extends up to ~16 eV.

ergy sequence of atomic-orbital contributions to the valence band. For increasing binding energy one finds first p_z-like states from cation (cation-cation bonding) and Se atoms at 0.8–1.5 eV from E_v. Then, in the order, p_x,p_y states (cation-Se bond), cation s-like states (antibonding, bonding cation-cation states), anion s-like states, and cation d-core levels. For GaS the sequence is also similar, but the characters of the first two features, peaks A and B, are mixed together. The energy position of the conduction-band features also shows similarities among the three materials. Four conduction-band structures d, f, g, and g' are present for all materials. Five more structures are only found for some of the materials (e, f', h, i, and l). The peaks d, e, f, g', and h have been predicted for GaSe by pseudopotential band-structure calculations[12,23] which predict a molecular character of the conduction band in this compound. The CIS spectra also offer a detailed explanation of previous ultraviolet reflectivity and electron-energy-loss data.

We would like to comment that the method of employing several different synchrotron-radiation photoemission-spectroscopy techniques in the same investigation underlines the limitations of the conventional EDC approach and shows promise of future developments. We are at present extending the investigation to different kinds of layer compounds and to adsorbates. In the latter case, several theoretical methods such as pseudopotential, tight binding, cluster, and other calculations are often equally good to treat the density of initial states and explain the conventional EDC's. However, data over a much wider spectral range below and above the Fermi level with photon polarization effects are a more stringent probe of the relative accuracy of these theoretical methods.

We would like to acknowledge helpful discussions with M. Schluter and H. Kasper. The cooperation of E. M. Rowe and R. A. Otte along with the entire staff of the Synchrotron Radiation Center, University of Wisconsin-Madison, has made these experiments possible. The Synchrotron Radiation Center is supported by the NSF under Grant No. DMR-74-15089.

*Supported in part by the Italian National Research Council-GNSM.

[1]D. E. Eastman, in *Vacuum Ultraviolet Radiation Physics*, edited by E. E. Koch (Pergamon-Vieweg, Braunschweig, 1974), p. 417.

[2]N. V. Smith (unpublished).

[3]M. Campagna, D. T. Pierce, F. Meier, K. Sattler, and H. C. Siegmann, in *Advances in Electronics and Electron Physics*, edited by L. L. Marton (Academic, New York, 1976), Vol. 41, p. 113.

[4]J. E. Rowe, Phys. Rev. Lett. 34, 398 (1974).

[5]J. E. Rowe, G. Margaritondo, H. Kaspers, and A. Baldereschi, Solid State Commun. 20, 921 (1976).

[6]M. Schluter, J. E. Rowe, G. Margaritondo, K. M. Ho, and M. L. Cohen, Phys. Rev. Lett. 37, 1632 (1976).

[7]D. E. Eastman and J. L. Freeouf, Phys. Rev. Lett. 33, 1601 (1974).

[8]G. J. Lapeyre, A. D. Baer, J. Hermanson, J. Anderson, J. A. Knapp, and P. L. Gobby, Solid State Commun. 15, 1601 (1974); G. J. Lapeyre, J. Anderson, P. L. Gobby, and J. A. Knapp, Phys. Rev. Lett. 33, 1290 (1974).

[9]G. J. Lapeyre and J. Anderson, Phys. Rev. Lett. 35, 117 (1975).

[10]F. Bassani and G. Pastori Parravicini, Nuovo Cimento B 50, 95 (1967).

[11]A. Baldereschi, K. Maschke, and M. Schluter, Helv. Phys. Acta 47, 434 (1974).

[12]M. Schluter and M. L. Cohen Phys. Rev. B 14, 424 (1976).

[13]P. Thiry, thesis (Université Pierre et Marie Curie, Paris, 1976) (unpublished).

[14]R. Mamy, L. Martin, G. Leveque, and C. Raisin, Phys. Status Solidi B 62, 201 (1974).

[15]V. V. Sobolev and V. I. Donetskich, Phys. Status Solidi B 45, K15 (1971).

[16]F. Bassani, D. L. Greenaway, and G. Fischer, in *Proceedings of the Seventh International Conference on the Physics of Semiconductors*, edited by M. Hulin,

(Academic, New York, 1964), p. 51.
1964), p. 51.
[17]E. Mooser and M. Schluter, Nuovo Cimento B 18, 174 (1973).
[18]W. Y. Liang, J. Phys. C 8, 1763 (1975).
[19]G. Margaritondo and J. E. Rowe, in *Proceedings of the 13th International Conference on the Physics of Semiconductors*, edited by F. G. Fumi (Marves, Roma, 1976), p. 138.
[20]D. R. Lloyd, C. M. Quinn, N. V. Richardson, and P. M. Williams, Phys. Commun. 1, 11 (1976).
[21]P. K. Larsen, G. Margaritondo, J. E. Rowe, M. Schluter, and N. V. Smith, Phys. Lett. A 58, 623 (1976).
[22]R. H. Williams, G. P. Williams, C. Norris, M. R. Howell, and I. H. Munro, J. Phys. C 7, L29 (1974); P. Thiry, R. Pincheaux, D. Dagneaux, and Y. Petroff, in *Proceedings of the 12th International Conference on the Physics of Semiconductors*, edited by M. Pilkuhn, Stuttgart 1974 (Teubner, Stuttgart, 1974), p. 2627; F. R. Shepherd and P. M. Williams, Phys. Rev. B 12, 5705 (1975); S. P. Kowalczyk, L. Ley, F. R. McFeely, and D. A. Shirley, Solid State Commun. 17, 463 (1976); R. H. Williams, I. T. McGovern, R. B. Murray, and H. Howells, Phys. Status Solidi B 73, 307 (1976).
[23]R. H. Williams, P. C. Kemeny, and L. Ley, Solid State Commun. 19, 495 (1976).
[24]J. C. Phillips, Phys. Rev. 188, 1225 (1968), and references therein.
[25]M. Schluter (private communication).
[26]However, a *complete* plane-wave character can be excluded since it would correspond to strong polarization effects while rotating the sample chamber in the geometry of Fig. 8 (inset) and we do not observe these effects.
[27]P. Soukiassan, J. Cazaux, and J. Perrin, Phys. Status Solidi B 66, 151 (1974).
[28]J. Perrin, J. Cazaux, and P. Soukiassan, J. Phys. (Paris) 35, C3-269 (1974).